Programmed death 1 protects from fatal circulatory failure during systemic virus infection of mice

Helge Frebel,[1] Veronika Nindl,[2] Reto A. Schuepbach,[3] Thomas Braunschweiler,[1] Kirsten Richter,[1] Johannes Vogel,[4] Carsten A. Wagner,[5] Dominique Loffing-Cueni,[6] Michael Kurrer,[7,8] Burkhard Ludewig,[2] and Annette Oxenius[1]

[1]Institute of Microbiology, ETH Zurich, 8093 Zurich, Switzerland
[2]Institute of Immunobiology, Cantonal Hospital St. Gallen, 9007 St. Gallen, Switzerland
[3]Surgical Intensive Care Medicine, University Hospital Zurich, 8091 Zurich, Switzerland
[4]Institute of Veterinary Physiology, [5]Institute of Physiology, and [6]Institute of Anatomy, [7]University of Zurich, 8006 Zurich, Switzerland
[8]Institute of Pathology Enge, 8027 Zurich, Switzerland

The inhibitory programmed death 1 (PD-1)–programmed death ligand 1 (PD-L1) pathway contributes to the functional down-regulation of T cell responses during persistent systemic and local virus infections. The blockade of PD-1–PD-L1–mediated inhibition is considered as a therapeutic approach to reinvigorate antiviral T cell responses. Yet previous studies reported that PD-L1–deficient mice develop fatal pathology during early systemic lymphocytic choriomeningitis virus (LCMV) infection, suggesting a host protective role of T cell down-regulation. As the exact mechanisms of pathology development remained unclear, we set out to delineate in detail the underlying pathogenesis. Mice deficient in PD-1–PD-L1 signaling or lacking PD-1 signaling in CD8 T cells succumbed to fatal CD8 T cell–mediated immunopathology early after systemic LCMV infection. In the absence of regulation via PD-1, CD8 T cells killed infected vascular endothelial cells via perforin-mediated cytolysis, thereby severely compromising vascular integrity. This resulted in systemic vascular leakage and a consequential collapse of the circulatory system. Our results indicate that the PD-1–PD-L1 pathway protects the vascular system from severe CD8 T cell–mediated damage during early systemic LCMV infection, highlighting a pivotal physiological role of T cell down-regulation and suggesting the potential development of immunopathological side effects when interfering with the PD-1–PD-L1 pathway during systemic virus infections.

CORRESPONDENCE
Annette Oxenius:
oxenius@micro.biol.ethz.ch

Abbreviations used: AST, aspartate aminotransferase; BAL, bronchoalveolar lavage; EB, Evan's blue; iNOS, inducible nitric oxide synthase; LCMV, lymphocytic choriomeningitis virus; NOs, nitric oxide species; PD-1, programmed death 1; PD-L1, programmed death ligand 1; p.i., post infection; TAT, thrombin–antithrombin.

The inhibitory programmed death 1 (PD-1)–programmed death ligand 1 (PD-L1) pathway was initially described to be involved in the induction and maintenance of peripheral tolerance, as PD-1–PD-L1 KO mice develop spontaneous autoimmune disease at the age of 6 mo (Nishimura et al., 1998, 1999, 2001; Nishimura and Honjo, 2001) and exacerbated induced autoimmunity (Dong et al., 2004; Latchman et al., 2004; Keir and Sharpe, 2005; Grabie et al., 2007; Hamel et al., 2010). Recent studies, however, suggest a novel role of the PD-1–PD-L1 pathway in the functional down-regulation of T cell responses during persistent viral, bacterial, and protozoan infections (Barber et al., 2006; Lázár-Molnár et al., 2010; Bhadra et al., 2011). This role was best studied in HIV infection in humans and in a mouse model of antiviral immunity during persistent systemic virus infections using lymphocytic choriomeningitis virus (LCMV; Wilson and Brooks, 2010).

PD-1 is expressed constitutively at high levels on CD4 and CD8 T cells during HIV, SIV, hepatitis C virus (HCV), and persistent LCMV infection and expression levels were shown to correlate with the degree of T cell dysfunction (Barber et al., 2006; Day et al., 2006; D'Souza et al., 2007; Blackburn et al.,

The Rockefeller University Press $30.00
J. Exp. Med. 2012 Vol. 209 No. 13 2485-2499
www.jem.org/cgi/doi/10.1084/jem.20121015

The Journal of Experimental Medicine

2009, 2010; Nakamoto et al., 2009; Velu et al., 2009). This persistently high expression level was observed to be driven by the sustained presence of viral antigen (Bucks et al., 2009; Mueller and Ahmed, 2009) and to significantly contribute to T cell down-regulation, as the antibody-mediated blockade of PD-1–PD-L1 signaling partially restored the function of previously unresponsive T cells (Barber et al., 2006; Day et al., 2006; Blackburn et al., 2008). As viral persistence is supposed to be intimately linked to the down-regulation of antiviral T cell responses, restoring T cell function through the blockade of PD-1 or its ligand PD-L1 is considered as a therapeutic approach to treat HIV and persistent HCV infections in humans (Urbani et al., 2008; Nakamoto et al., 2009; Velu et al., 2009; Chiodi, 2010).

However, the increasing number of studies reporting PD-1–PD-L1–mediated down-regulation of T cell responses during persistent bacterial or viral infections suggests a potentially vital role of this inhibitory pathway. A growing body of evidence from mouse model systems indicates that the impairment of the PD-1–PD-L1 pathway can cause aggravated if not lethal pathology during distinct infections (Iwai et al., 2003; Barber et al., 2006, 2011; Lázár-Molnár et al., 2010; Mueller et al., 2010; Phares et al., 2010; Chen et al., 2011). Barber et al. (2006) showed that PD-L1 KO mice succumb to a systemic LCMV infection within 7 d, indicating a protective role of this pathway during the early phase of systemic infection. Likewise, Mueller et al. (2010) described a rapid development of fatal pathology in systemically infected mice that lacked PD-L1 expression on nonhematopoietic cells. Yet the pathophysiological mechanisms that contribute to pathology development under conditions of PD-1–PD-L1 deficiency have remained elusive. It also remained unknown which specific nonhematopoietic cell type required PD-L1 expression to prevent fatal pathology.

In this study, we investigated the role of the PD-1–PD-L1 pathway during the early phase of systemic LCMV infection. We determined the impact of impaired PD-1–PD-L1 signaling on early virus-directed immune responses and elucidated the immunological processes that lead to fatality. We found that pathology was driven by virus-specific CD8 T cells and depended on the expression of perforin. During systemic infection, endothelial cells strongly up-regulated PD-L1 expression on their cell surface which inhibited the killing of infected endothelial cells by virus-specific CD8 T cells. PD-1 deficiency or the Ab-mediated blockade of PD-L1 facilitated endothelial cell killing, leading to increased vascular permeability and ultimately to circulatory collapse.

RESULTS

PD-1 KO mice succumb to CD8 T cell–mediated pathology during systemic LCMV infection

A previous study indicated a lethal outcome of systemic LCMV infection in PD-L1–deficient mice (Barber et al., 2006). To confirm that this fatal pathology was the result of deficient signaling via the PD-1–PD-L1 pathway, we examined the course of systemic LCMV infection in PD-1 (receptor) KO mice. As reported for PD-L1 KO mice, PD-1 KO mice also succumbed to a systemic LCMV clone 13 infection (10^6 pfu) with similar kinetics (Fig. 1 A). This also applied to a systemic infection (10^6 pfu) with the more virulent strain LCMV docile. In contrast, PD-1 KO mice did not succumb to a rapidly controlled LCMV infection when infected with 10^2 pfu of LCMV docile. Thus, lethal pathology only developed during a systemic infection which, in the following experiments, was established by infecting with 10^6 pfu of LCMV docile.

As a quantitative parameter to determine disease onset and progression, we longitudinally measured the core temperature of WT C57BL/6 and PD-1 KO mice after LCMV infection. Concurrent with the emergence of visible disease symptoms (hunched back, ruffled fur, and reduced motoric activity), PD-1 KO mice exhibited a sharp decrease of core temperature from days 5 to 6 post infection (p.i.) which was not observed in asymptomatic WT mice (Fig. 1 B). As the above experiments implied the impairment of PD-1–PD-L1 signaling to cause pathology development, we speculated that the administration of blocking anti–PD-L1 (αPD-L1) antibody would also evoke fatal pathology in systemically infected WT mice. Although untreated WT mice remained asymptomatic, αPD-L1–treated WT mice displayed the same disease symptoms and kinetics that were observed in infected PD-1 KO mice (Fig. 1 C).

As the inhibitory PD-1–PD-L1 pathway was reported to contribute to T cell down-regulation early after systemic LCMV infection (Barber et al., 2006), we investigated a possible role of the antiviral T cell response in pathology development. The emergence of disease symptoms simultaneously with the onset of the antiviral T cell response also suggested an involvement of virus-specific T cells. We found that depleting CD8 T cells entirely prevented disease development of infected PD-1 KO mice, whereas the depletion of CD4 T cells had no effect (Fig. 1 D). These results indicated that PD-1 KO mice succumbed to a CD8 T cell–mediated pathology. A comparison of CD8 T cell responses in WT and PD-1 KO mice on day 6 p.i. revealed increased numbers of LCMV-specific CD8 T cells in the spleens of PD-1 KO mice and increased inflammatory infiltration of the periphery (liver) with virus-specific CD8 T cells, total CD8 T cells, CD4 T cells, and inflammatory polymorphonuclear cells (unpublished data). Consistent with an enhanced antiviral CD8 T cell response, PD-1 KO mice exhibited modestly improved virus control (unpublished data). PD-1 deficiency also resulted in elevated serum levels of the proinflammatory cytokines IFN-γ, TNF, and IL-6 (Fig. 1 E) and in moderately elevated serum concentrations of the liver aspartate aminotransferase (AST) compared with infection-matched WT mice (Fig. 1 F). In addition, only PD-1 KO mice suffered from focal hepatocellular necrosis in the form of visible lesion in liver tissue (unpublished data).

PD-1 deficiency renders virus-specific CD8 T cells pathogenic

To investigate the role of PD-1 exclusively in virus-specific CD8 T cells, we crossed TCR transgenic P14 mice with PD-1 KO mice. This enabled us to obtain a PD-1–deficient

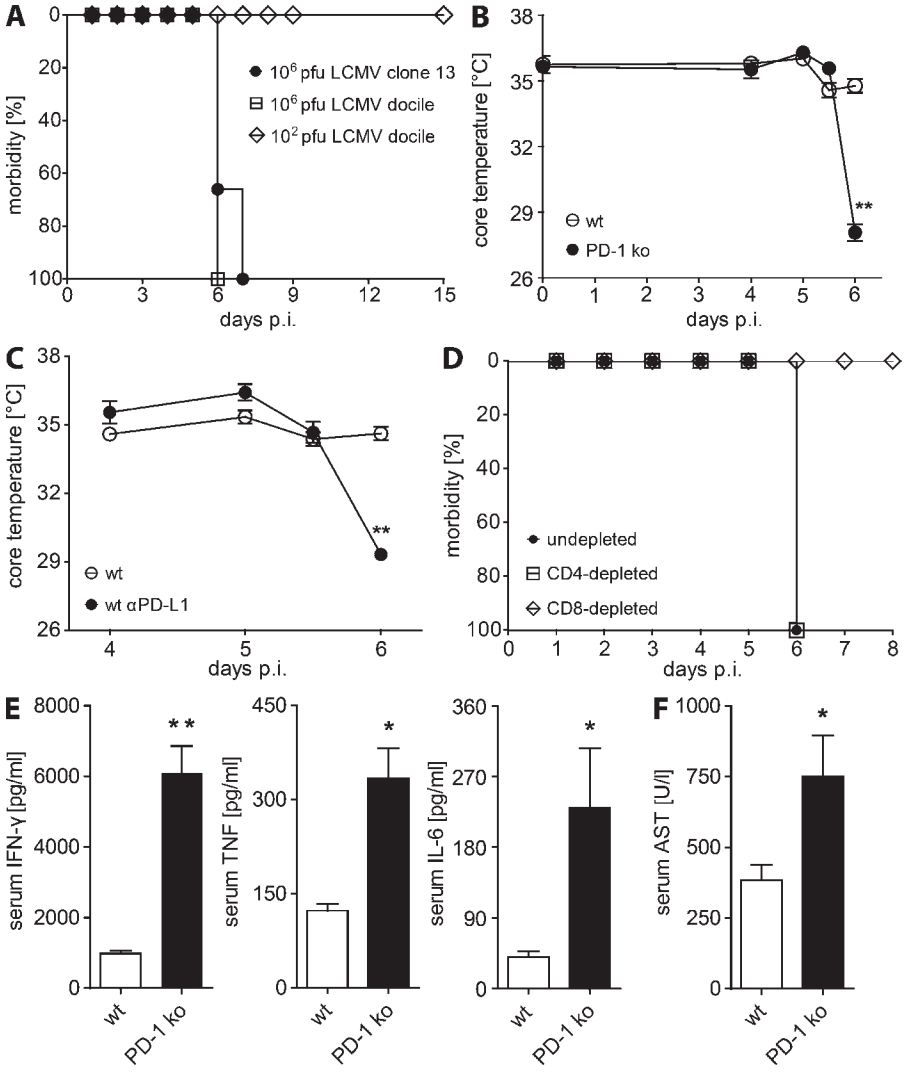

Figure 1. PD-1 KO mice develop fatal CD8 T cell–dependent pathology during early systemic LCMV infection. (A) PD-1 KO mice were infected with 10^6 pfu LCMV clone 13, 10^6 pfu LCMV docile, or 10^2 pfu LCMV docile and monitored for morbidity (hunched back, ruffled fur, and reduced motoric activity). (B and C) Core temperatures were measured in WT and PD-1 KO mice (B), untreated and αPD-L1–treated WT mice (C). (D) Morbidity was monitored in undepleted and CD8 T cell– or CD4 T cell–depleted PD-1 KO mice at the indicated times after infection with 10^6 pfu LCMV docile. (E) Cytokine concentrations in the sera of WT and PD-1 KO mice were analyzed on day 6 after 10^6 pfu LCMV docile infection. A–E: $n = 3$–4 mice per group. Means ± SEM from one representative of two experiments are shown. (F) Liver AST concentrations in the sera of WT and PD-1 KO mice were determined on day 6 after infection. WT, $n = 8$ mice; KO, $n = 7$ mice. Means ± SEM from two pooled experiments are shown. *, $P < 0.05$; **, $P < 0.01$ (unpaired two-tailed Student's *t* test).

monoclonal CD8 T cell population that was specific for the LCMV epitope GP33 (P14 cells). We adoptively transferred WT mice either with 10^4 PD-$1^{-/-}$ or PD-$1^{+/+}$ P14 cells, followed by a systemic LCMV infection. On day 6 p.i., mice were sacrificed and compared for the expansion and functional capacity of transferred CD8 T cell populations. We found that PD-$1^{-/-}$ P14 cells expanded to higher percentages and total numbers in the spleen compared with PD-$1^{+/+}$ P14 cells (Fig. 2 A). Moreover, the percentage of IFN-γ–producing cells within transferred P14 cells was significantly higher when these were PD-1 deficient. This, in combination with a higher mean fluorescence intensity of IFN-γ in transferred PD-$1^{-/-}$ P14 cells (Fig. 2 B), suggested an increased functional capacity of PD-1–deficient virus-specific CD8 T cells on day 6 p.i. Accordingly, we found PD-$1^{-/-}$ P14-transferred WT mice to display higher serum concentrations of IFN-γ (Fig. 2 C) and modestly improved virus control in the spleen compared with PD-$1^{+/+}$ P14-transferred WT mice (Fig. 2 D). The enhanced antiviral response of PD-1–deficient CD8 T cells was also reflected by increased serum concentrations of AST and the formation of focal necrotic liver lesions (Fig. 2 E) as described above in PD-1 KO mice (Fig. 1 F). Moreover, the transfer of 2.5×10^4 PD-$1^{-/-}$ P14 cells to WT mice led to the development of fatal pathology on day 6 p.i. as seen in PD-1 KO mice (Fig. 2 F), with pathology development being more severe when transferring higher numbers of PD-$1^{-/-}$ P14 cells. This was in sharp contrast to PD-$1^{+/+}$ P14-transferred WT mice, which did not develop any disease symptoms when transferred with 2.5×10^4 P14 cells. These data demonstrate that selective PD-1 deficiency in virus-specific CD8 T cells results in significantly enhanced functional capacity, which leads to the development of fatal pathology on day 6 after systemic LCMV infection.

Perforin and nonhematopoietic H-2D^b expression are required for pathology development

We next aimed at determining the cellular effector mechanisms underlying the pathogenicity of PD-1 KO CD8 T cells during early systemic LCMV infection. As the T cell effector cytokines IFN-γ and TNF were measured in significantly

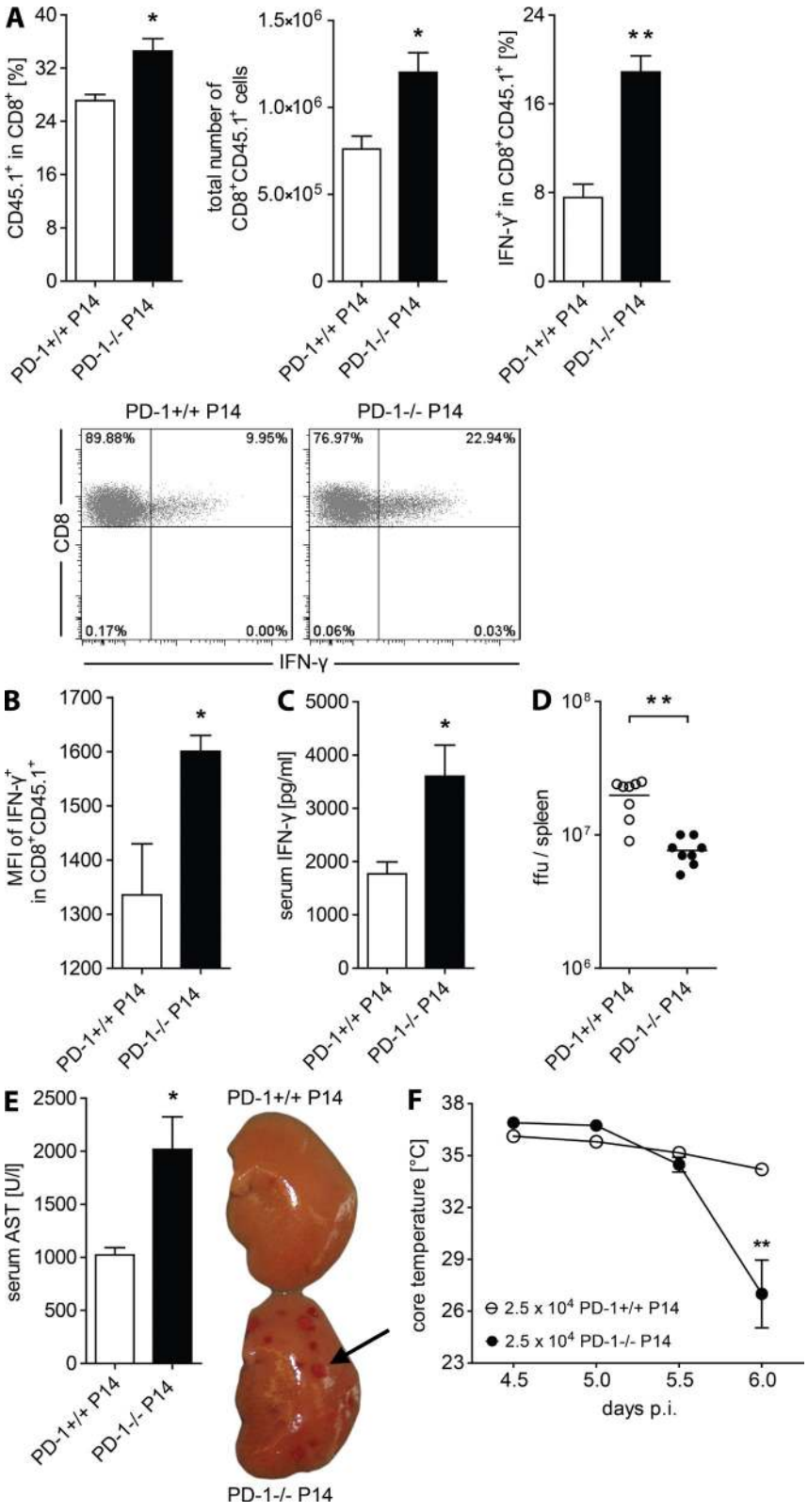

Figure 2. PD-1–deficient virus-specific CD8 T cells are more functional and pathogenic. (A and B) WT mice were transferred with 10^4 PD-$1^{+/+}$ or PD-$1^{-/-}$ P14 cells, followed by 10^6 pfu LCMV docile infection on the next day. On day 6 p.i., percentages and total numbers of splenic P14 cells were determined. The percentage of IFN-γ–producing cells in transferred P14 cells (A) and the mean fluorescence intensity of IFN-γ (B) were measured after restimulation with GP33 peptide. $n = 3–4$ mice per group. Means ± SEM from one representative of two experiments are shown. (C) Serum concentrations of IFN-γ were analyzed on day 6 after infection. $n = 3–4$ mice per group. Means ± SEM from one representative of two experiments are shown. (D) Splenic virus titers were analyzed on day 6 after infection. $n = 8$ mice per group. Means ± SEM from two pooled experiments are shown. (E) Serum levels of liver AST were determined and photos of PBS-perfused liver lobes were taken on day 6 p.i. The arrow indicates a focal necrotic liver lesion. $n = 3–4$ mice per group. Means ± SEM from one representative of two experiments and photos from representative mice from one of two experiments are shown. (F) WT mice were transferred with 2.5×10^4 PD-$1^{+/+}$ or PD-$1^{-/-}$ P14 cells, followed by 10^6 pfu LCMV docile infection and core temperature was monitored. $n = 4$ mice per group. Means ± SEM from one representative of two experiments are shown. *, $P < 0.05$; **, $P < 0.01$ (unpaired two-tailed Student's t test).

increased concentrations (6.2- and 2.7-fold, respectively) in the sera of PD-1 KO mice compared with infection-matched WT mice, we hypothesized these cytokines to contribute to pathology. To test this, we conducted antibody-mediated neutralizations of IFN-γ and TNF in PD-1 KO mice during systemic infection. As shown in Fig. 3 A, the double neutralization of IFN-γ and TNF did not prevent pathology development but rather showed a trend toward accelerated disease

progression. We had also measured elevated levels of IL-6 (5.7-fold) in the sera of PD-1 KO mice. Araki et al. (2010) reported a contribution of elevated IL-6 and TNF levels to fatal, CD8 T cell–dependent pathology in calcineurin inhibitor-treated WT mice after acute LCMV infection. We thus investigated if a blockade of the IL-6 receptor combined with TNF neutralization could prevent fatality in PD-1 KO mice. This also failed to prevent disease development, which was reflected by the strong decline of core temperature in treated PD-1 KO mice (Fig. 3 B).

Apart from the secretion of soluble effectors, CD8 T cells drive virus-infected cells into apoptosis, which is crucial for LCMV control in vivo (Kägi et al., 1994). We determined the impact of CD8 T cell cytotoxicity on pathology development by treating WT and perforin-deficient mice (PKOB) with αPD-L1. Although αPD-L1–treated WT mice displayed the characteristic decline of core temperature on day 6 p.i., the core temperature in αPD-L1–treated PKOB mice remained constant as in untreated PKOB mice (Fig. 3 C). Importantly, we measured comparable percentages of splenic GP33-specific CD8 T cells in αPD-L1–treated WT and PKOB mice, indicating that the expansion of virus-specific CD8 T cells was not impaired in perforin-deficient mice (unpublished data). Based on the severity and fast kinetics of pathology development, we speculated that recognition of virally infected nonhematopoietic cells by cytotoxic T cells would be involved. To test this hypothesis, we generated bone marrow chimeric mice that lacked H-2D^b expression on nonhematopoietic cells through reconstituting the hematopoietic compartment of lethally irradiated H-2D^b KO mice with WT bone marrow cells (WT→H-2D^b KO). As a control, lethally irradiated WT mice were reconstituted with WT bone marrow (WT→WT). To circumvent the problem of impaired thymic development of H-2D^b–restricted T cells in WT→H-2D^b KO chimeric mice, 2.5×10^4 PD-1$^{-/-}$ P14 cells were transferred to all mice, followed by systemic LCMV infection. As illustrated in Fig. 3 D, WT→WT chimeric mice developed clear disease symptoms on day 6 after systemic infection in contrast to WT→H-2D^b KO chimeric mice that only exhibited a slight decrease of core temperature. These results indicated perforin and nonhematopoietic H-2D^b, but not IFN-γ, TNF, or IL-6, to be involved in pathology development.

PD-L1 blockade enhances endothelial cell killing by virus-specific CD8 T cells

Based on the observation that CD8 T cells, perforin, and nonhematopoietic H-2D^b expression were crucial for fatal pathology, we screened the animals for severe tissue damage in vital organs which could be made responsible for fatality. However, histological analysis of the liver, lung, kidney, heart, and brain did not reveal signs of notable organ damage in the form of apoptotic or necrotic regions apart from focal hepatocellular lesions and liver steatosis (unpublished data). The only moderate increase in AST levels (Fig. 1 F), comparable serum albumin concentrations, and normal blood glucose concentrations in WT and PD-1 KO mice excluded acute liver failure (not depicted). We concluded that fatal pathology did not develop as a result of critical tissue damage in the above-mentioned vital organs.

Several studies described a strong up-regulation of PD-L1 expression on vascular endothelial cells under inflammatory conditions (Eppihimer et al., 2002; Rodig et al., 2003; Grabie et al., 2007). We speculated that vascular endothelial

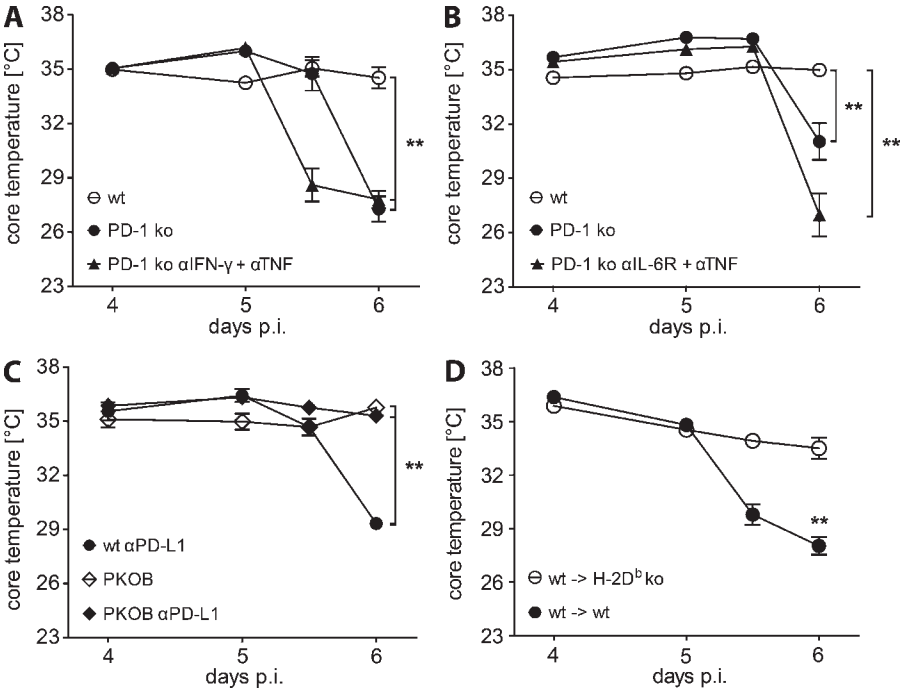

Figure 3. Perforin and nonhematopoietic H-2D^b expression are required for pathology development. (A and B) Core temperatures were measured in WT mice, PD-1 KO mice, and αIFN-γ + αTNF–treated PD-1 KO mice (A) or αIL-6R + αTNF-treated PD-1 KO mice (B) after 10^6 pfu LCMV docile infection. (C) Core temperatures were monitored in untreated WT and PKOB mice and in αPD-L1–treated WT and PKOB mice after infection. A–C: n = 3–4 mice per group. Means ± SEM from one representative of two experiments are shown. **, $P < 0.01$ (unpaired two-tailed Student's t test). (D) WT→WT and WT→H-2D^b KO chimeric mice were transferred with 2.5×10^4 PD-1$^{-/-}$ P14 cells, followed by 10^6 pfu LCMV docile infection and monitoring of core temperature. WT→WT, n = 9 mice per group; WT→H-2D^b KO, n = 12 mice per group. Means ± SEM from two pooled experiments are shown. **, $P < 0.01$ (unpaired two-tailed Student's t test).

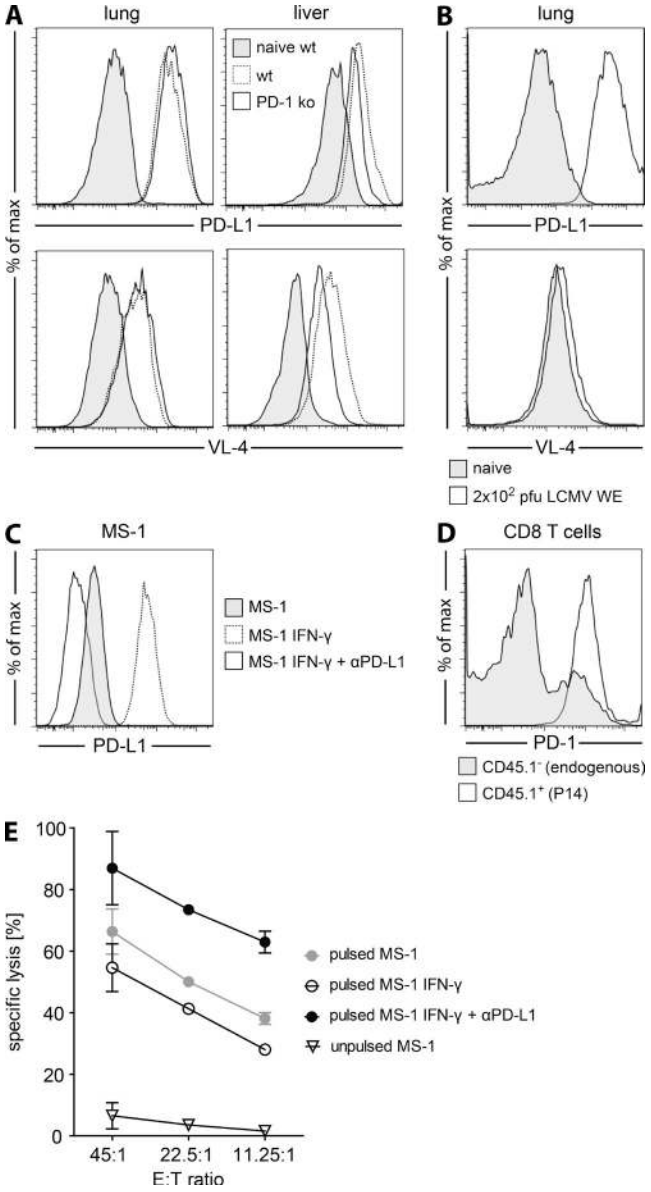

Figure 4. Endothelial PD-L1 expression inhibits CD8 T cell–mediated killing. (A) $CD31^+CD144^+$ cells from lungs and livers of naive WT, infected WT, and infected PD-1 KO mice were analyzed for PD-L1 expression and LCMV infection (VL-4 staining) on day 6 after 10^6 pfu LCMV docile infection. Histograms depict data from one representative of two analyzed mice per group. Data from one representative of three experiments are shown. (B) Lung $CD31^+CD144^+$ cells of naive and 10^2 pfu LCMV WE–infected WT mice were analyzed for PD-L1 expression and LCMV infection (VL-4 staining) on day 6 p.i. Histograms depict data from one mouse each. Data from one representative of two experiments are shown. (C) Untreated, IFN-γ–treated, and IFN-γ + αPD-L1–treated MS-I cells were analyzed for PD-L1 expression and pulsed with GP33+NP396 peptide to serve as target cells in a chromium release assay. (D) PD-1 expression levels of endogenous CD8 T cells and transferred P14 cells were determined on day 6 after systemic infection. C and D: histograms depict data from one representative of two experiments. (E) CD8 T cells were purified from four P14-transferred mice on day 6 p.i. and mixed with chromium-labeled, antigen-pulsed MS-I cells at the indicated effector to target ratios. Chromium release was analyzed in duplicates. Means ± SEM from one representative of three experiments are shown.

cells might up-regulate PD-L1 under the inflammatory conditions of a systemic LCMV infection and thereby inhibit the killing of LCMV-infected endothelium by activated, PD-1–expressing CD8 T cells. In contrast, PD-1–deficient CD8 T cells would not be inhibited by PD-L1 and thus effectively kill LCMV-infected vascular endothelial cells. To test this hypothesis, the expression level of PD-L1 on liver and lung endothelial cells was analyzed ex vivo on day 6 p.i. We detected a strong up-regulation of PD-L1 on endothelial cells from both organs in infected WT and PD-1 KO mice compared with endothelial cells from naive WT mice (Fig. 4 A). Furthermore, we found the vast majority of liver and lung endothelial cells to be infected with LCMV on day 6 p.i., indicated by strong intracellular staining with the LCMV nucleoprotein-specific antibody VL-4 (Fig. 4 A).

To assess whether endothelial cells up-regulate PD-L1 in response to inflammatory mediators or as the result of a direct infection with LCMV, WT mice were infected with 10^2 pfu of LCMV WE. After 6 d, this rapidly controlled infection was localized to the spleen, leaving lung endothelial cells uninfected (Fig. 4 B). However, the uninfected endothelial cells exhibited a significantly increased expression level of PD-L1 compared with naive WT mice, indicating that the up-regulation of PD-L1 expression was independent of a direct infection but rather a response to systemic inflammatory mediators during LCMV infection.

We now examined the impact of PD-1–PD-L1 signaling on endothelial cell killing by CD8 T cells from systemically infected mice. The mouse endothelial cell line MS-1 was left untreated or cultured in the presence of IFN-γ for 48 h, which led to a pronounced up-regulation of PD-L1 on the cell surface (Fig. 4 C). Next, cells were pulsed with LCMV peptides (GP33+NP396) in the presence or absence of blocking αPD-L1 antibody and subsequently co-cultured with CD8 T cells purified from the spleens of P14-transferred WT mice on day 6 p.i. Consistent with previous results (Barber et al., 2006), LCMV-specific CD8 T cells had strongly up-regulated PD-1 expression in response to systemic LCMV infection (Fig. 4 D). We found that the killing of antigen-pulsed endothelial cells was clearly influenced by PD-1–PD-L1 signaling, with modest killing of PD-L1–expressing endothelial cells which was markedly increased (twofold on average) when PD-1–PD-L1 signaling was blocked (Fig. 4 E).

To directly verify whether killing of infected endothelial cells occurred in vivo, lung tissue of naive and systemically infected mice was isolated and examined for apoptotic endothelium by immunofluorescence microscopy. Although no apoptotic endothelial cells were detected in naive mice, apoptosis was prevalent in endothelium of WT and PD-1 KO mice 5–6 d p.i. (Fig. 5 A). A quantitative analysis revealed significantly elevated numbers of apoptotic endothelial cells in lung sections of infected PD-1 KO mice compared

with WT mice (Fig. 5 B). Importantly, impaired PD-1–PD-L1 signaling had a stronger impact on endothelial cell killing in the presence of perforin than in PKOB mice, further corroborating the perforin-dependent endothelial cell apoptosis in vivo (Fig. 5 B). We also assessed the impact of impaired PD-1–PD-L1 signaling on the killing of infected endothelial cells by flow cytometry. Consistent with the above results, we found decreased total numbers of endothelial cells in the lungs of αPD-L1–treated WT mice compared with untreated WT mice on day 6 p.i. (Fig. 5 C). In conclusion, these data demonstrate that endothelial cells from WT and PD-1 KO mice are permissive for LCMV during systemic infection and up-regulate PD-L1 under inflammatory conditions. This PD-L1 up-regulation inhibited life-threatening killing of virus antigen–presenting endothelial cells by activated CD8 T cells which was restored by PD-L1 blockade.

Vascular integrity is compromised in PD-1 KO mice

Endothelial cells represent the physiological barrier between the vascular space and the organ interstitium. Thus, killing of endothelial cells can compromise vascular integrity. We compared the vascular permeability in the kidney, liver, lung, and brain in infected PD-1 KO mice to the permeability in WT mice. As a surrogate for vascular barrier function, we determined the amount of albumin-bound Evan's blue (EB) recovered from the interstitium of each organ 20 min after i.v. injection of the dye. As shown in Fig. 6 A, PD-1 deficiency caused elevated levels of vascular permeability in all analyzed organs on day 6 p.i., with the most pronounced increase of extracted EB in the lung (Fig. 6 B). Vascular damage uncovers procoagulant structures, such as tissue factor–bearing cells and connective tissue, which trigger vascular coagulation (Cines et al., 1998; Dahlbäck, 2000). As evidence for an activated clotting system, we found increased concentrations of thrombin–antithrombin (TAT) complexes in infected animals that were most pronounced in PD-1 KO mice (Fig. 6 C). Severely decreased platelet counts in infected PD-1 KO as compared with WT mice further supported a more pronounced procoagulant stage in infected PD-1–deficient mice (Fig. 6 D).

We next determined whether factors we had shown to be dispensable or required for pathology development had similar effects on vascular permeability. Consistent with the above results (Fig. 3 B), a simultaneous blockade of IL-6R and neutralization of TNF did not reduce the elevated levels of vascular permeability in PD-1 KO mice (Fig. 6 E). We, however, observed a significant reduction of vascular permeability in the lungs and livers of αPD-L1–treated PKOB mice compared with αPD-L1–treated WT mice (Fig. 6 F). Particularly in the lung, the αPD-L1–mediated increase of vascular leakage was reduced by >66% in the absence of perforin. Moreover, PD-$1^{-/-}$ P14 cell-mediated vascular permeabilization was completely abrogated in the lungs of WT→H-$2D^b$ KO chimeric mice compared with WT→WT chimeric mice, which exhibited high vascular permeability (Fig. 6 G). Together, these results indicate a significant role of perforin-mediated cell lysis and nonhematopoietic H-$2D^b$ expression in the loss of vascular integrity particularly in the lungs of PD-1 KO mice during early systemic LCMV infection.

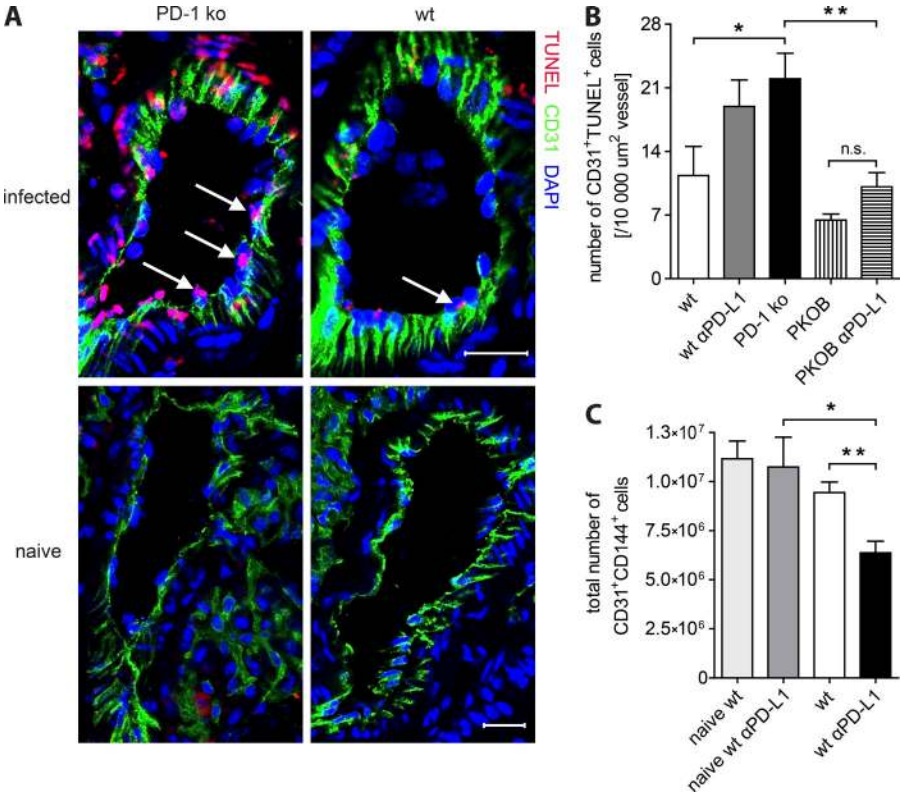

Figure 5. Pulmonary endothelial cells are driven into apoptosis after systemic LCMV infection. (A) In situ analysis of lung sections from naive and infected WT and PD-1 KO mice on days 5–6 after 10^6 pfu LCMV docile infection. Representative immunofluorescence stainings with the indicated antibodies are shown. The arrows indicate apoptotic endothelial cells as identified by TUNEL⁺CD31⁺ cells. $n = 7$ mice. Bars, 20 µm. (B) Quantification of CD31⁺TUNEL⁺ cells in immunofluorescence stainings of pulmonary vessels on day 5 p.i. Numbers of CD31⁺TUNEL⁺ cells were normalized to vessel areas and two to three sections per mouse were considered for quantification. WT, $n = 4$ mice; wt αPD-L1, $n = 4$ mice; PD-1 KO, $n = 3$ mice; PKOB, $n = 3$ mice; PKOB αPD-L1, $n = 3$ mice. Means ± SEM from two pooled experiments are shown. n.s.: not significant. (C) Total numbers of lung CD31⁺CD144⁺ cells were determined in naive and infected WT and αPD-L1–treated WT mice on day 6 p.i. $n = 5$–6 mice per group. Means ± SEM from two pooled experiments are shown. *, $P < 0.05$; **, $P < 0.01$ (unpaired two-tailed Student's t test).

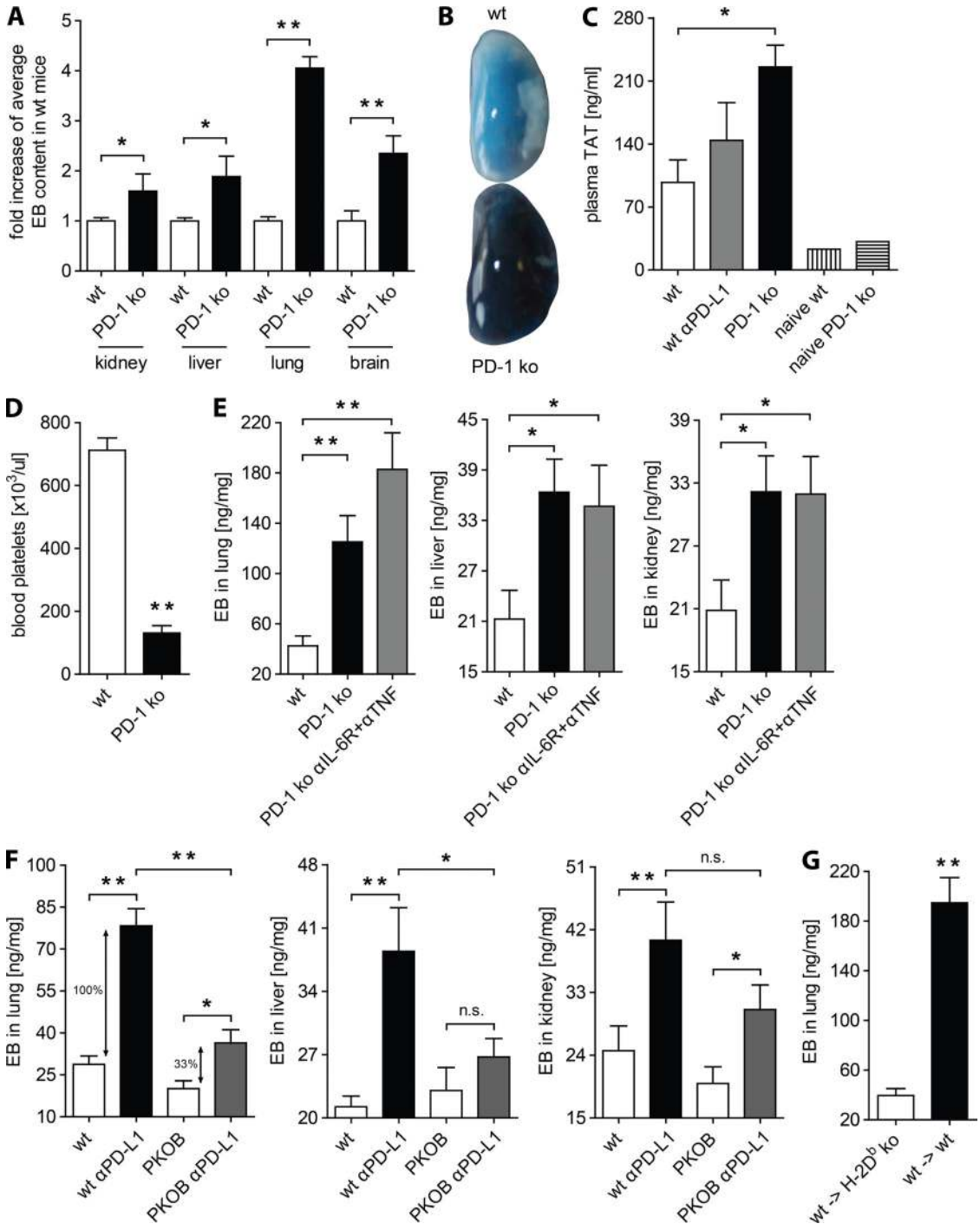

Figure 6. PD-1 KO mice exhibit systemically increased vascular permeability. (A) EB was injected i.v. to WT and PD-1 KO mice on day 6 after 10^6 pfu LCMV docile infection and EB extravasation was analyzed in the kidney, liver, lung, and brain. The mean EB concentration in organs of WT mice was normalized to 1. Values in PD-1 KO mice were calculated accordingly. WT, n = 10 mice; KO, n = 5–6 mice. Means ± SEM from three pooled experiments are shown. (B) Photos of PBS-perfused lung lobes from WT and PD-1 KO mice were taken after EB injection on day 6 after infection. Photos from representative mice from one of two experiments are shown. (C) TAT plasma concentrations were determined in naive WT and PD-1 KO mice and infected WT, αPD-L1–treated WT, and PD-1 KO mice on day 6 p.i. Infected, n = 3–4 mice per group; naive, n = 1 mouse per group. Means ± SEM from one representative of two experiments are shown. (D) Total numbers of blood platelets were determined in WT and PD-1 KO mice on day 6 after infection. n = 2–4 mice per group. Means ± SEM from one representative of two experiments are shown. (E) EB extravasation was determined in the kidney, liver, and lung of infected WT, PD-1 KO, and αIL-6R + αTNF–treated PD-1 KO mice on day 6 after systemic infection. n = 6–8 mice per group. Means ± SEM from two pooled experiments are shown. (F) EB extravasation was analyzed in the kidney, liver, and lung of untreated WT and PKOB mice and αPD-L1–treated WT and PKOB mice on day 6 p.i. n = 6–8 mice per group. Means ± SEM from two pooled experiments are shown. n.s.: not significant. (G) EB extravasation

PD-1 KO mice suffer from pulmonary edema and severe hypotension

Increasing vascular permeability can cause edema formation in the organ interstitium (Goldenberg et al., 2011; Matthay and Zemans, 2011). As significantly higher amounts of EB were extracted from PD-1 KO lungs than from WT lungs, we compared the extent of pulmonary edema formation on day 6 p.i. The wet/dry weight ratio of an organ increases with accumulating interstitial fluid. We observed significantly higher wet/dry weight ratios for lungs isolated from diseased PD-1 KO mice than from WT mice (Fig. 7 A). An additional breach of the endothelial barrier between vascular and alveolar space leads to the accumulation of plasma in the airways. This would result in elevated total protein concentrations in the bronchoalveolar lavage (BAL). Although protein concentrations were comparable in naive WT and PD-1 KO mice, infected PD-1 KO mice exhibited significantly more total protein in the BAL than infected WT mice (Fig. 7 B). This independently pointed toward the development of pulmonary edema in PD-1 KO mice in addition to the elevated wet/dry weight ratios. The increase of albumin in the BAL of PD-1 KO mice indicated exudation and not transudation as underlying mechanism (Fig. 7 C). Furthermore, the lungs of infected PD-1 KO mice exhibited focal intraalveolar hemorrhage (Fig. 7 D), and histological sections of nonperfused lung tissue confirmed the extensive formation of interstitial edema with few regions of alveolar edema that were absent in sections of infected WT mice (Fig. 7 F). As previous results had suggested vascular permeabilization to be significantly dependent on perforin expression (Fig. 6 F), BAL albumin concentrations were also determined in untreated and αPD-L1–treated WT and PKOB mice. In contrast to treated WT mice, treated PKOB mice did not exhibit increased albumin concentrations in the BAL, whereas untreated mice exhibited comparably low levels (Fig. 7 E).

We next asked if pulmonary edema formation in PD-1 KO mice might impair respiratory gas exchange. An analysis of arterial blood revealed that gas exchange at rest was sufficient and peripheral oxygen delivery was not impaired in PD-1 KO mice (Fig. 7 G). Considering the systemic nature and degree of vessel permeability in infected PD-1 KO mice, the consequences of increased vascular permeability on the circulatory system were investigated. We found that the mean arterial pressure in PD-1 KO mice was reduced to critical levels (∼50 mmHg) on day 6 p.i., whereas the mean pressure in WT mice was within the normal range (100–120 mmHg; Fig. 7 H). A longitudinal analysis showed a progressive and rapid decrease of blood pressure in PD-1 KO and αPD-L1–treated WT mice starting on late day 5 p.i. and reaching critical levels on day 6 p.i. (Fig. 7 I). This was in sharp contrast to WT and CD8-depleted PD-1 KO mice which exhibited physiologically normal values during the entire measurement. Thus, the absence of PD-1–PD-L1–mediated inhibition led to a CD8 T cell–dependent systemic increase of vascular permeability with a consecutive hypovolemic shock.

In conclusion, our data demonstrate a pivotal role of the PD-1–PD-L1 pathway in the functional down-regulation of virus-specific CD8 T cells during early systemic LCMV infection. This down-regulation prevents vascular damage caused by the killing of virus-infected endothelial cells, which rapidly culminates in fatal circulatory failure.

DISCUSSION

Besides its acknowledged role in tolerance and autoimmunity, increasing evidence is found for an immunoregulatory function of the PD-1–PD-L1 pathway in cancer immunology and infectious diseases (Driessens et al., 2009;Virgin et al., 2009; Brown et al., 2010; Francisco et al., 2010). We now describe a critical inhibitory role of this pathway for protecting the vascular system from CD8 T cell–mediated damage during systemic virus infection of mice. PD-1 deficiency or PD-L1 blockade both led to fatal pathology early after systemic LCMV infection. Pathology development was driven by PD-1 KO CD8 T cells, which exhibited significantly enhanced functionality compared with WT CD8 T cells. Although IFN-γ, TNF, and IL-6R signaling were dispensable for pathology development, perforin-mediated effector functions and nonhematopoietic H-2D^b expression were crucially involved. We found that compromised PD-1–PD-L1 signaling enhanced endothelial cell killing by virus-specific CD8 T cells, leading to reduced endothelial cell numbers and increased vascular permeability. Consequently, infected PD-1 KO mice suffered from pulmonary edema and critical hypotension. These results suggest that PD-1–PD-L1–mediated inhibition of cytotoxic T cell activity protects from self-inflicted damage of the circulatory system during early systemic viral infection.

The fact that pathology is clearly CD8 T cell dependent is consistent with results from Mueller et al. (2010), who demonstrated that the absence of PD-L1 in nonhematopoietic cells resulted in fatality after systemic LCMV infection. However, we further delineated this mechanism by showing that PD-1 deficiency in CD8 T cells was sufficient for the development of fatal pathology and that this was linked to perforin-mediated effector functions. The above study also demonstrated that the absence of PD-L1 on hematopoietic cells led to fatal pathology, albeit with delayed kinetics. This very likely resulted from the documented increase in numbers and function of virus-specific CD8 T cells caused by the absence of down-regulation by PD-L1–deficient hematopoietic cells. Although our in vitro killing assays indicated that PD-L1 expression on endothelial cells confers a significant

was analyzed in the lungs of 2.5 × 10^4 PD-1$^{-/-}$ P14 cell-transferred WT→WT and WT→H-2D^b KO chimeric mice on day 6 p.i. WT→WT, n = 7 mice per group; WT→H-2D^b KO, n = 12 mice per group. Means ± SEM from two pooled experiments are shown. *, P < 0.05; **, P < 0.01 (unpaired two-tailed Student's t test).

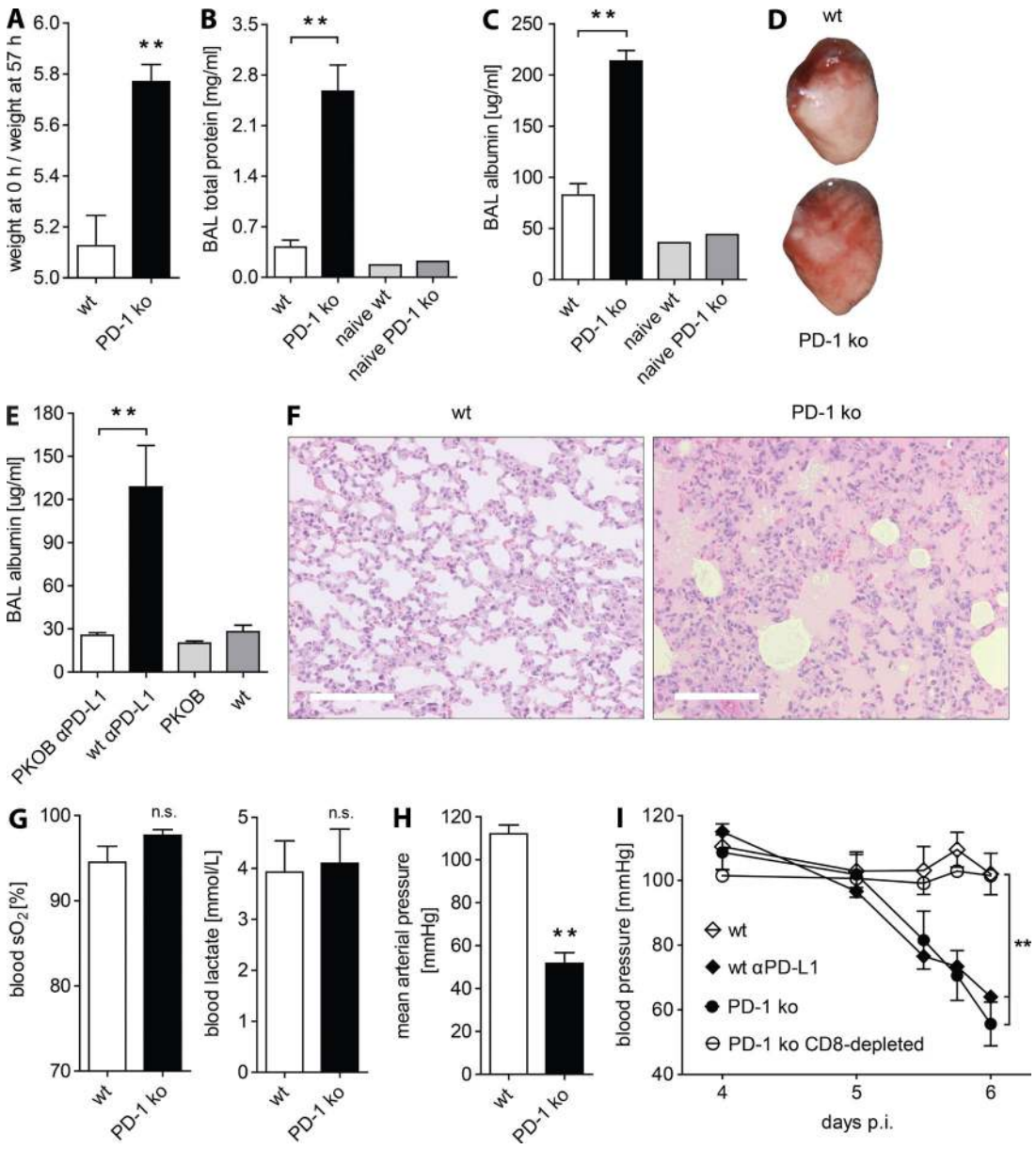

Figure 7. PD-1 KO mice develop pulmonary edema and severe hypotension. (A) Wet/dry weight ratios of whole lungs from WT and PD-1 KO mice were determined on day 6 after 10^6 pfu LCMV docile infection. n = 3–4 mice per group. Means ± SEM from one representative of two experiments are shown. (B and C) Total protein concentrations (B) and albumin concentrations (C) were determined in the BAL supernatant of naive and infected WT and PD-1 KO mice on day 6 p.i. Infected, n = 6–7 mice per group; naive, n = 1 mouse per group. Means ± SEM from two pooled experiments are shown. (D and F) Photos were taken of nonperfused, PFA-fixed lung lobes (D) and H&E-stained lung sections (F) from WT and PD-1 KO mice on day 6 after infection. Photos from representative mice from one of two experiments are shown. Bars, 150 µm. (E) Albumin concentrations were determined in the BAL supernatant of untreated and αPD-L1–treated WT and PKOB mice on day 6 p.i. Treated, n = 7–8 mice per group; untreated, n = 3 mice per group. Means ± SEM from two pooled experiments are shown. (G) O_2 saturation and lactate concentration in arterial blood were measured in WT and PD-1 KO mice on day 6 p.i. n = 4 mice per group. Means ± SEM from one representative of two experiments are shown. n.s.: not significant. (H) Mean arterial blood pressure was determined in WT and PD-1 KO mice on day 6 p.i. n = 4 mice per group. Means ± SEM from one representative of two experiments are shown. (I) Blood pressure was determined in WT, αPD-L1–treated WT, PD-1 KO, and CD8 T cell–depleted PD-1 KO mice between days 4 and 6 after infection. n = 4 mice per group. Means ± SEM are shown. **, $P < 0.01$ (unpaired two-tailed Student's t test).

degree of protection against lysis by PD-1–expressing CD8 T cells, this protection is not complete. Hence, a strong increase in numbers and function of virus-specific CD8 T cells in mice with PD-L1 deficiency on hematopoietic cells might overcome the threshold of PD-L1–conferred protection in endothelial cells. Unlike speculations in previous studies of immunopathology in PD-1–PD-L1 KO mice (Mueller et al., 2010; Phares et al., 2010; Chen et al., 2011), we found that

the proinflammatory cytokines IFN-γ, TNF, and IL-6 were not required for pathology development. Yet a potential caveat of these results is that cytokines cannot be neutralized to 100% by the application of blocking antibodies.

In agreement with results of Rodig et al. (2003), blocking of PD-L1 clearly enhanced the killing of antigen-pulsed endothelial cells by in vivo–activated CD8 T cells in vitro. The inhibition of endothelial cell killing through PD-L1 upregulation might be particularly potent during systemic LCMV infection, as virus-specific CD8 T cells exhibit a high expression level of PD-1. Furthermore, our observations are supported by reports of ameliorated CD8 T cell–dependent organ damage by endothelial PD-L1 expression during experimentally induced myocarditis (Grabie et al., 2007), transplant vasculopathy (Bolinger et al., 2010), and viral hepatitis (Iwai et al., 2003).

The increased extent of interstitial EB extravasation in multiple organs showed that PD-1 deficiency led to elevated vascular permeability during systemic LCMV infection. This was most prominent in the lung, perhaps because this organ has the largest endothelial area or because lung endothelium is more affected than other endothelia. The more modest extent of EB extravasation in organs of αPD-L1–treated PKOB mice suggested a significant role of perforin in the increase of vascular permeability. However, the increase detected in the absence of perforin expression also indicated a contribution of additional factors. Potential mechanisms might be Fas/FasL- and TRAIL/DR4/5-mediated killing of endothelial cells or alterations of endothelial cell adhesion through soluble mediators other than IFN-γ, TNF, or IL-6. Yet the level of vascular permeability observed in αPD-L1–treated PKOB mice was insufficient to cause fatal pathology. The important role of perforin-mediated cell lysis in vascular permeabilization is in contrast to pathologies with similar clinical pictures, for example, sepsis, where inflammatory mediators were found to drive pathogenesis (Tracey et al., 1987; Leon et al., 1998; Shresta et al., 2006). Furthermore, pathogenic PD-$1^{-/-}$ P14 cells failed to increase vascular permeability in the lungs of nonhematopoietic H-$2D^b$–deficient mice, whereas mice expressing nonhematopoietic H-$2D^b$ exhibited clearly increased vascular permeability. This observation indicated a central role of nonhematopoietic antigen presentation in the permeabilization of the pulmonary vasculature. A potential caveat of this experiment is the additional endogenous H-$2D^b$–restricted CD8 T cell response in WT→WT chimeric mice which is absent in WT→H-$2D^b$ chimeras. However, endogenous T cells are subjected to strong PD-1–PD-L1–mediated down-regulation and likely exert a negligible impact on pathology development compared with the transferred 2.5×10^4 PD-$1^{-/-}$ P14 cells.

As CD8 T cell–mediated recruitment of polymorphonuclear cells was suggested to contribute to fatal CNS pathology after intracranial LCMV infection (Kim et al., 2009), we considered a role of polymorphonuclear cells in the development of the pathology described here. A major effector mechanism of polymorphonuclear cells is the production of cytotoxic and vasodilatative nitric oxide species (NOs). The activity of inducible nitric oxide synthase (iNOS), an enzyme which is required for the generation of polymorphonuclear cell–derived NOs, was described to significantly contribute to hepatic virus control after systemic LCMV infection and increased cerebral iNOS transcription coincided with elevated serum levels of nitrite/nitrate during lethal intracranial LCMV infection (Campbell et al., 1994; Campbell, 1996; Guidotti et al., 2000). To test for a possible role of polymorphonuclear cell–derived NOs in pathology development, we treated iNOS-deficient mice with αPD-L1 followed by systemic LCMV infection. As seen with WT mice, the blockade of PD-1–PD-L1 signaling induced pathology development in infected iNOS-deficient mice on day 6 p.i., which indicated the dispensability of polymorphonuclear cell–derived NOs for pathology development (unpublished data). Moreover, the depletion of a major polymorphonuclear cell type, neutrophils, with a Ly-6G–targeting antibody did not prevent pathology development in infected PD-1 KO mice (unpublished data). Although our data strongly support a CD8 T cell–mediated mechanism of immunopathology, other cell types, such as NK cells or NKT cells, also bear the potential of perforin-mediated cell lysis. Yet treatment of infected PD-1 KO mice with depleting αNK1.1 antibody did not prevent pathology development (unpublished data).

The loss of vascular integrity in systemically infected PD-1 KO mice caused the formation of pulmonary edema. Despite edematous septa and scattered intraalveolar fluid accumulation, no evidence of impaired pulmonary gas exchange was found at rest. A more prolonged leakage of fluid into the alveolar space might be required to overcome the lung's overcapacity at rest to significantly impact gas exchange. Although leaking plasma into organ interstitium can impair organ function, it can also affect the circulatory system. Increased vascular permeability and intravascular coagulation during endotoxic sepsis or hemorrhagic fever are associated with critical hypotension (Srikiatkhachorn, 2009; Goldenberg et al., 2011). A longitudinal measurement of the arterial blood pressure revealed a CD8 T cell–mediated progressive decrease of arterial blood pressure in diseased PD-1 KO and αPD-L1–treated WT mice to levels which do not allow for sufficient organ perfusion.

The application of PD-1–PD-L1 pathway-blocking antibodies is considered as a therapeutic approach to reinvigorate down-regulated T cell responses during advanced systemic infections (Barber et al., 2006; Day et al., 2006; Lafon et al., 2008; Chiodi, 2010; Bhadra et al., 2011; Telcian et al., 2011), vaccinations (Ha et al., 2008), and antitumor treatments (Brahmer et al., 2010; Kline and Gajewski, 2010; Mkrtichyan et al., 2011). The release of PD-1–PD-L1–mediated immune inhibition can hold promise for specific therapeutic settings but might also bear considerable detrimental potential. For instance, the blockade of another member of the CD28 superfamily, CTLA-4, in the context of cancer treatments, caused diverse immune-related side effects like colitis/diarrhea, dermatitis, hepatitis, and endocrinopathies (Berman et al., 2010; Di Giacomo et al., 2010). Moreover, a recent clinical study

investigating the benefit of PD-1 blockade in the context of cancer treatment showed adverse events including pneumonitis (Brahmer et al., 2012; Topalian et al., 2012). Our results now highlight important aspects that might be worth considering for therapeutic approaches targeting the PD-1–PD-L1 pathway; although an increase of T cell function by PD-L1 blockade during the advanced phase of systemic LCMV infection improves virus control apparently devoid of clinically relevant immunopathology (Barber et al., 2006), PD-L1 blockade in the early phase of the same infection is lethal. This suggests divergent roles of PD-1–PD-L1–mediated immunoinhibition during distinct phases of the infection, being host-protective during the early phase but promoting pathogen persistence during the advanced phase. Accordingly, the timing of PD-L1 blockade might be crucial to avoid adverse side effects. Our data further indicate that the pathogen's biology and pathogen-specific aspects of the immune response have to be taken into consideration. Pathology could only be induced using LCMV inoculum doses that led to the systemic infection of endothelial cells at the time of extensive T cell expansion. Therefore, it is likely that the systemic nature of the infection, as well as a viral tropism which includes endothelial cells, is required to evoke the described pathology of the vascular system. This view is supported by a recent study describing a new infection model of a further endothelial cell–tropic Arenavirus, Lassa virus, where the infection of WT mice caused increased vascular permeability and edema formation with a strict CD8 T cell dependence of the pathology (Flatz et al., 2010). Interestingly, Lassa virus and LCMV share their cellular receptor, α-Dystroglycan, which is expressed by endothelial cells (Kunz et al., 2001, 2005). Moreover, Lassa virus was shown to infect human and nonhuman primate endothelial cells (Lukashevich et al., 1999; Hensley et al., 2011), whereas the infection of nonhuman primates is associated with coagulopathy and hypotension (Fisher-Hoch et al., 1987). As the systemic LCMV infection of WT mice already caused a mild increase of vascular permeability and intravascular coagulation compared with naive WT mice, it can be speculated that PD-L1 blockade aggravates a clinically silent pathology during systemic LCMV infection which might have comparable pathophysiological mechanisms to those observed during Lassa virus infection.

In summary, we identified a mechanism through which the inhibitory PD-1–PD-L1 pathway protects vascular integrity during early systemic LCMV infection by down-modulating cytotoxic CD8 T cell effector functions. Our findings provide relevant insights for the development of therapeutic approaches that aim at intervening with the PD-1–PD-L1 pathway and potentially other negative regulatory pathways.

MATERIALS AND METHODS

Ethics statement. This study was performed in strict accordance with the guidelines of the animal experimentation law (SR 455.163; TVV) of the Swiss Federal Government. The protocol was approved by Cantonal Veterinary Office of the canton of Zurich, Switzerland (Permit number 146/2008).

Mice and infections. The following mouse strains were housed and bred in specific pathogen-free facilities at the Institute of Microbiology, ETH Zurich, or at the RCC Füllinsdorf, Switzerland: C57BL/6 mice, PD-1 KO (*Pdcd1*$^{-/-}$) mice (Nishimura et al., 1998), PKOB mice (Kägi et al., 1994), H-2D^{b} KO mice (Pascolo et al., 1997), and CD45.1^{+} P14 mice. All KO and transgenic mice were on a C57BL/6 background with >10 backcrosses. C57BL/6 mice were also purchased from Elevage Janvier. Transgenic CD45.1^{+} P14 mice expressing a TCR specific for the LCMV epitope GP33-41 were described previously (Pircher et al., 1990). CD45.1^{+} P14 mice were crossed with PD-1 KO mice to generate PD-1$^{-/-}$CD45.1^{+} P14 mice. All animals were used at 6–14 wk of age. This also applied to PD-1 KO mice that had been reported to spontaneously develop mild autoimmune disease only with advanced age (6 mo or older; Nishimura et al., 1999). The LCMV isolates clone 13, docile, and WE were provided by R.M. Zinkernagel (University Hospital, Zurich, Switzerland). For LCMV infection, mice were injected i.v. with 200 or 10^{6} pfu of respective strains. The viral peptides GP33–41 (GP33; KAVYNFATM) and NP396–404 (NP396; FQPQNGQFI) were purchased from NeoMPS (Strasbourg, France).

Core temperature and experiment endpoint. Mice were anesthetized for 90 s with isoflurane (3.5% in oxygen) and the core temperature was measured in the rectum using a rectal temperature probe of a Homeothermic Blanket Control Unit (Harvard Apparatus). In accordance with veterinary office regulations, mice that exhibited a >15% decrease of the steady-state rectal temperature (~35.5°C) were considered to be irreversibly diseased and euthanized immediately.

Tetramers, antibodies, neutralizations, blockades, and depletions. APC-conjugated peptide–MHC class I tetrameric complexes were produced as previously described (Altman et al., 1996). All antibodies for flow cytometric analysis were purchased from BioLegend (LucernaChem) or BD. For double neutralization of IFN-γ and TNF, 500 µg αIFN-γ (clone: R4-6A2 or XMG1.1; BioXCell) and 500 µg αTNF (clone: XT3.11; BioXCell) were injected i.p. on days 1, 3, and 5 p.i. For simultaneous neutralization of TNF and blockade of IL-6R, 660 µg αIL-6R (clone: 15A7; BioXCell) and 500 µg αTNF (clone: XT3.11; BioXCell) were injected i.p. on days 1, 3, and 5 p.i. For T cell depletion, mice were injected i.p. with 200 µg αCD4 (clone: YTS 191.1) or with 200 µg αCD8 (clone: YTS169) every second day starting on day 3 p.i. For PD-L1 blockade, 200 µg αPD-L1 (clone: 10F.9G2; BioXCell) were injected i.p. daily from days 0 to 5 p.i.

Stimulation of lymphocytes and flow cytometry. Lymphocytes were isolated from organs of PBS-perfused mice and stimulated with 1 µg/ml GP33 + 1 µg/ml NP396 peptide in the presence of 10 µg/ml Brefeldin A (Sigma-Aldrich) for 5 h at 37°C. For analysis of degranulation, 1 µl αCD107a was added during the stimulation. Surface staining was conducted for 30 min at 4°C. Afterward, cells were fixed and permeabilized in 500 µl 2× FACS Lyse (BD) with 0.05% Tween 20 (Sigma-Aldrich) for 10 min at room temperature. The cells were washed and intracellular staining was conducted for 30 min at room temperature. Cells were washed and resuspended in PBS containing 1% PFA (Sigma-Aldrich). Flow cytometric analysis was performed using an LSRII flow cytometer in combination with FACSDiva software (both BD). Raw data were analyzed using FlowJo software (Tree Star).

Cell isolation, adoptive transfers, and cell line. CD8 T cells were purified from spleen single cell suspensions using MACS microbeads for positive selection of CD8 T cells in combination with LS columns (Miltenyi Biotec) according to the manufacturer's instructions. 1×10^{4} or 2.5×10^{4} purified CD8 T cells isolated from naive PD-1$^{+/+}$CD45.1^{+} P14 or PD-1$^{-/-}$CD45.1^{+} P14 mice were adoptively transferred into naive recipient mice on day 1 p.i. The endothelial cell line MS-I was obtained from R.A. Schuepbach.

Analysis of serum cytokine, serum liver AST, serum albumin, BAL albumin, BAL total protein, and blood glucose concentrations. Serum cytokine concentrations were measured using Cytometric Bead Array kits (BD) according to the manufacturer's instructions. The obtained raw data

were analyzed with FCAP Array software (Soft Flow Inc.). Serum liver AST and serum or BAL albumin levels were measured at the Clinical Chemistry Department of the University Hospital, Zurich, Switzerland. Total protein concentrations in the BAL were measured via Bradford assay. Blood glucose levels were determined using an Accu-Chek Aviva Nano (Roche).

Histopathology. Multiple liver lobes were taken from PBS-perfused mice, embedded in Tissue-Tek OCT compound (Sakura) and snap-frozen in liquid nitrogen. Sections were cut in a cryostat and stained with H&E. For lung histology, multiple lobes were taken from nonperfused mice and fixed in PBS buffered formalin. Fixed tissue was embedded in paraffin and sections were stained with H&E at the Cantonal Hospital, St. Gallen, Switzerland. All sections were examined by a pathologist blinded to the specific experimental conditions.

Immunofluorescence. Isolated nonperfused lungs were immersed in BSS, snap frozen in liquid nitrogen and cut in a cryostat. For cryopreservation, 10-µm tissue sections were fixed in acetone for 10 min. After thawing, tissue sections were air dried and TUNEL staining was performed according to the manufacturer's protocol for the In situ Cell Death Detection kit TMR red (Roche). For surface stainings, sections were incubated with αCD31 Alex-648 (LucernaChem) in a humidified chamber for 2 h at room temperature and nuclei were visualized with DAPI. Images were acquired on the confocal microscope LSM 710 (Carl Zeiss) and processed using the ZEN 2009 (Carl Zeiss) software and DRAW X4 (Corel).

Virus loads and chromium release assay. Virus loads were determined in the spleen, one lung lobe, and one brain hemisphere as previously described (Battegay et al., 1991). For chromium release assays, four WT mice were transferred with 2.5×10^4 P14 cells and infected with 10^6 pfu LCMV docile on the next day. On day 6 p.i., splenic CD8 T cells were purified and used as effector cells. As target cells, MS-I cells were cultured with and without 100 U/ml IFN-γ for 48 h and labeled with 100 µCi of $Na_2{}^{51}CrO_4$ (Hartmann Analytic) for 90 min at 37°C. At the same time, cells were pulsed with the LCMV peptides GP33 (1 µg/ml) + NP396 (1 µg/ml) and incubated with 30 µg/ml αPD-L1 (clone: 10F.9G2; BioXCell), where indicated. Cells were washed twice and co-cultured with effector cells at given ratios in duplicates in a 96-well plate for 6 h at 37°C. Spontaneous release (SR) was measured with target cells only in triplicate and maximum release (MR) with target cells plus 2N HCl in triplicate. After incubation, supernatant was taken from each well and chromium release was measured using a Packard Cobra Auto Gamma Counter (PerkinElmer). Specific lysis was calculated according to the following formula: $\%\ \text{specific lysis} = (CPM_{Sample} - CPM_{SR})/(CPM_{MR} - CPM_{SR}) \times 100$.

Bone marrow chimeric mice. Chimeric mice were generated by transferring 5×10^6 bone marrow cells isolated from C57BL/6 mice to recipients that had been lethally irradiated (950 rad) 1 d before the transfer. During the first 14 d of reconstitution, mice were treated with a 1:250 dilution of Borgal 24% (Intervet) in drinking water. Chimeric mice were used for experiments 6 wk after reconstitution.

Analysis of vascular permeability. Mice were injected i.v. with 200 µl of 0.5% EB in PBS. After 20 min, mice were lethally anesthetized and transcardially perfused with 10 ml PBS to remove intravascular EB. One liver lobe, one kidney, two lung lobes, and one brain hemisphere were excised and weighed. To extract extravascular EB, each organ was incubated in 1 ml formamide overnight at 56°C. The amount of extracted EB was determined by a photometrical analysis of the EB-formamide solution at 620 nm and by comparing to an EB standard curve.

Plasma TAT concentrations and platelet counts. Plasma TAT concentrations were analyzed using the Enzygnost Tat micro kit (Siemens Healthcare) according to the manufacturer's instructions. Blood platelet counts were determined at the Hematology Department of the Cantonal Hospital, Winterthur, Switzerland.

Wet/dry weight ratio. The thorax of lethally anesthetized mice was opened and the hilum of the right lung was closed immediately with surgical filament. The prepared right lung was removed and weighed (wet weight). After drying for >30 h at 60°C, the lung was weighed (dry weight) and the wet/dry weight ratio was calculated.

Analysis of blood oxygenation and arterial blood pressure. Arterial blood gases and blood pressure were analyzed in conscious and resting mice. While anesthetized with isoflurane (2–2.5% in oxygen), mice were implanted with a polyethylene catheter into the left femoral artery. After applying two drops of 2% lidocaine solution (Streuli) to the wound, it was closed and mice were allowed to recover from anesthesia for 15 min while continuously recording blood pressure with a piezoelectric pressure transducer and a PowerLab system (ADInstruments). 100 µl blood was drawn from the catheter for blood gas and lactate measurements (AVL700 Radiometer). Mice were euthanized by cervical dislocation after drawing blood. Kinetics of the systolic arterial blood pressure were measured noninvasively using the BP-2000 Blood Pressure Analysis System (Visitech Systems).

Statistics. Statistical significance was determined with an unpaired two-tailed Student's *t* test in Prism (GraphPad Software).

We would like to thank Nathalie Oetiker and Franziska Wagen (ETH Zurich), as well as Karin Eugster and Eva Allgäuer (Cantonal Hospital St. Gallen), for technical assistance. In addition, we thank Bernhard Odermatt (University Hospital Zurich) for the analysis of histological sections and Daniel Binder (Cantonal Hospital Winterthur) for determining blood cell counts. We also thank Mrs. Frebber from Siemens Healthcare for providing the Enzygnost Tat micro kit. We are grateful for the analysis of AST and albumin concentrations in serum and BAL conducted by the Department of Clinical Chemistry, University Hospital Zurich.

This work was funded by the ETH Zurich and the Swiss National Science Foundation (grant no. 310030-113947 to A. Oxenius).

The authors declare no financial or commercial conflict of interest.

Submitted: 11 May 2012
Accepted: 13 November 2012

REFERENCES

Altman, J.D., P.A. Moss, P.J. Goulder, D.H. Barouch, M.G. McHeyzer-Williams, J.I. Bell, A.J. McMichael, and M.M. Davis. 1996. Phenotypic analysis of antigen-specific T lymphocytes. *Science*. 274:94–96. http://dx.doi.org/10.1126/science.274.5284.94

Araki, K., S. Gangappa, D.L. Dillehay, B.T. Rouse, C.P. Larsen, and R. Ahmed. 2010. Pathogenic virus-specific T cells cause disease during treatment with the calcineurin inhibitor FK506: implications for transplantation. *J. Exp. Med*. 207:2355–2367. http://dx.doi.org/10.1084/jem.20100124

Barber, D.L., E.J. Wherry, D. Masopust, B. Zhu, J.P. Allison, A.H. Sharpe, G.J. Freeman, and R. Ahmed. 2006. Restoring function in exhausted CD8 T cells during chronic viral infection. *Nature*. 439:682–687. http://dx.doi.org/10.1038/nature04444

Barber, D.L., K.D. Mayer-Barber, C.G. Feng, A.H. Sharpe, and A. Sher. 2011. CD4 T cells promote rather than control tuberculosis in the absence of PD-1-mediated inhibition. *J. Immunol*. 186:1598–1607. http://dx.doi.org/10.4049/jimmunol.1003304

Battegay, M., S. Cooper, A. Althage, J. Bänziger, H. Hengartner, and R.M. Zinkernagel. 1991. Quantification of lymphocytic choriomeningitis virus with an immunological focus assay in 24- or 96-well plates. *J. Virol. Methods*. 33:191–198. http://dx.doi.org/10.1016/0166-0934(91)90018-U

Berman, D., S.M. Parker, J. Siegel, S.D. Chasalow, J. Weber, S. Galbraith, S.R. Targan, and H.L. Wang. 2010. Blockade of cytotoxic T-lymphocyte antigen-4 by ipilimumab results in dysregulation of gastrointestinal immunity in patients with advanced melanoma. *Cancer Immun*. 10:11.

Bhadra, R., J.P. Gigley, L.M. Weiss, and I.A. Khan. 2011. Control of *Toxoplasma* reactivation by rescue of dysfunctional CD8+ T-cell response via PD-1-PDL-1 blockade. *Proc. Natl. Acad. Sci. USA*. 108:9196–9201. http://dx.doi.org/10.1073/pnas.1015298108

Blackburn, S.D., H. Shin, G.J. Freeman, and E.J. Wherry. 2008. Selective expansion of a subset of exhausted CD8 T cells by alphaPD-L1 blockade. *Proc. Natl. Acad. Sci. USA*. 105:15016–15021. http://dx.doi.org/10.1073/pnas.0801497105

Blackburn, S.D., H. Shin, W.N. Haining, T. Zou, C.J. Workman, A. Polley, M.R. Betts, G.J. Freeman, D.A. Vignali, and E.J. Wherry. 2009. Coregulation of CD8+ T cell exhaustion by multiple inhibitory receptors during chronic viral infection. *Nat. Immunol.* 10:29–37. http://dx.doi.org/10.1038/ni.1679

Blackburn, S.D., A. Crawford, H. Shin, A. Polley, G.J. Freeman, and E.J. Wherry. 2010. Tissue-specific differences in PD-1 and PD-L1 expression during chronic viral infection: implications for CD8 T-cell exhaustion. *J. Virol.* 84:2078–2089. http://dx.doi.org/10.1128/JVI.01579-09

Bolinger, B., D. Engeler, P. Krebs, S. Miller, S. Firner, M. Hoffmann, D.C. Palmer, N.P. Restifo, Y. Tian, P.A. Clavien, and B. Ludewig. 2010. IFN-gamma-receptor signaling ameliorates transplant vasculopathy through attenuation of CD8+ T-cell-mediated injury of vascular endothelial cells. *Eur. J. Immunol.* 40:733–743. http://dx.doi.org/10.1002/eji.200939706

Brahmer, J.R., C.G. Drake, I. Wollner, J.D. Powderly, J. Picus, W.H. Sharfman, E. Stankevich, A. Pons, T.M. Salay, T.L. McMiller, et al. 2010. Phase I study of single-agent anti-programmed death-1 (MDX-1106) in refractory solid tumors: safety, clinical activity, pharmacodynamics, and immunologic correlates. *J. Clin. Oncol.* 28:3167–3175. http://dx.doi.org/10.1200/JCO.2009.26.7609

Brahmer, J.R., S.S. Tykodi, L.Q. Chow, W.J. Hwu, S.L. Topalian, P. Hwu, C.G. Drake, L.H. Camacho, J. Kauh, K. Odunsi, et al. 2012. Safety and activity of anti-PD-L1 antibody in patients with advanced cancer. *N. Engl. J. Med.* 366:2455–2465. http://dx.doi.org/10.1056/NEJMoa1200694

Brown, K.E., G.J. Freeman, E.J. Wherry, and A.H. Sharpe. 2010. Role of PD-1 in regulating acute infections. *Curr. Opin. Immunol.* 22:397–401. http://dx.doi.org/10.1016/j.coi.2010.03.007

Bucks, C.M., J.A. Norton, A.C. Boesteanu, Y.M. Mueller, and P.D. Katsikis. 2009. Chronic antigen stimulation alone is sufficient to drive CD8+ T cell exhaustion. *J. Immunol.* 182:6697–6708. http://dx.doi.org/10.4049/jimmunol.0800997

Campbell, I.L. 1996. Exacerbation of lymphocytic choriomeningitis in mice treated with the inducible nitric oxide synthase inhibitor aminoguanidine. *J. Neuroimmunol.* 71:31–36. http://dx.doi.org/10.1016/S0165-5728(96)00129-4

Campbell, I.L., A. Samimi, and C.S. Chiang. 1994. Expression of the inducible nitric oxide synthase. Correlation with neuropathology and clinical features in mice with lymphocytic choriomeningitis. *J. Immunol.* 153:3622–3629.

Chen, Y., S. Wu, G. Guo, L. Fei, S. Guo, C. Yang, X. Fu, and Y. Wu. 2011. Programmed death (PD)-1-deficient mice are extremely sensitive to murine hepatitis virus strain-3 (MHV-3) infection. *PLoS Pathog.* 7:e1001347. http://dx.doi.org/10.1371/journal.ppat.1001347

Chiodi, F. 2010. New therapy to revert dysfunctional antibody responses during HIV-1 infection. *J. Clin. Invest.* 120:3810–3813. http://dx.doi.org/10.1172/JCI44872

Cines, D.B., E.S. Pollak, C.A. Buck, J. Loscalzo, G.A. Zimmerman, R.P. McEver, J.S. Pober, T.M. Wick, B.A. Konkle, B.S. Schwartz, et al. 1998. Endothelial cells in physiology and in the pathophysiology of vascular disorders. *Blood.* 91:3527–3561.

D'Souza, M., A.P. Fontenot, D.G. Mack, C. Lozupone, S. Dillon, A. Meditz, C.C. Wilson, E. Connick, and B.E. Palmer. 2007. Programmed death 1 expression on HIV-specific CD4+ T cells is driven by viral replication and associated with T cell dysfunction. *J. Immunol.* 179:1979–1987.

Dahlbäck, B. 2000. Blood coagulation. *Lancet.* 355:1627–1632. http://dx.doi.org/10.1016/S0140-6736(00)02225-X

Day, C.L., D.E. Kaufmann, P. Kiepiela, J.A. Brown, E.S. Moodley, S. Reddy, E.W. Mackey, J.D. Miller, A.J. Leslie, C. DePierres, et al. 2006. PD-1 expression on HIV-specific T cells is associated with T-cell exhaustion and disease progression. *Nature.* 443:350–354. http://dx.doi.org/10.1038/nature05115

Di Giacomo, A.M., M. Biagioli, and M. Maio. 2010. The emerging toxicity profiles of anti-CTLA-4 antibodies across clinical indications. *Semin. Oncol.* 37:499–507. http://dx.doi.org/10.1053/j.seminoncol.2010.09.007

Dong, H., G. Zhu, K. Tamada, D.B. Flies, J.M. van Deursen, and L. Chen. 2004. B7-H1 determines accumulation and deletion of intrahepatic CD8(+) T lymphocytes. *Immunity.* 20:327–336. http://dx.doi.org/10.1016/S1074-7613(04)00050-0

Driessens, G., J. Kline, and T.F. Gajewski. 2009. Costimulatory and coinhibitory receptors in anti-tumor immunity. *Immunol. Rev.* 229:126–144. http://dx.doi.org/10.1111/j.1600-065X.2009.00771.x

Eppihimer, M.J., J. Gunn, G.J. Freeman, E.A. Greenfield, T. Chernova, J. Erickson, and J.P. Leonard. 2002. Expression and regulation of the PD-L1 immunoinhibitory molecule on microvascular endothelial cells. *Microcirculation.* 9:133–145.

Fisher-Hoch, S.P., S.W. Mitchell, D.R. Sasso, J.V. Lange, R. Ramsey, and J.B. McCormick. 1987. Physiological and immunologic disturbances associated with shock in a primate model of Lassa fever. *J. Infect. Dis.* 155:465–474. http://dx.doi.org/10.1093/infdis/155.3.465

Flatz, L., T. Rieger, D. Merkler, A. Bergthaler, T. Regen, M. Schedensack, L. Bestmann, A. Verschoor, M. Kreutzfeldt, W. Brück, et al. 2010. T cell-dependence of Lassa fever pathogenesis. *PLoS Pathog.* 6:e1000836. http://dx.doi.org/10.1371/journal.ppat.1000836

Francisco, L.M., P.T. Sage, and A.H. Sharpe. 2010. The PD-1 pathway in tolerance and autoimmunity. *Immunol. Rev.* 236:219–242. http://dx.doi.org/10.1111/j.1600-065X.2010.00923.x

Goldenberg, N.M., B.E. Steinberg, A.S. Slutsky, and W.L. Lee. 2011. Broken barriers: a new take on sepsis pathogenesis. *Sci. Transl. Med.* 3:ps25. http://dx.doi.org/10.1126/scitranslmed.3002011

Grabie, N., I. Gotsman, R. DaCosta, H. Pang, G. Stavrakis, M.J. Butte, M.E. Keir, G.J. Freeman, A.H. Sharpe, and A.H. Lichtman. 2007. Endothelial programmed death-1 ligand 1 (PD-L1) regulates CD8+ T-cell mediated injury in the heart. *Circulation.* 116:2062–2071. http://dx.doi.org/10.1161/CIRCULATIONAHA.107.709360

Guidotti, L.G., H. McClary, J.M. Loudis, and F.V. Chisari. 2000. Nitric oxide inhibits hepatitis B virus replication in the livers of transgenic mice. *J. Exp. Med.* 191:1247–1252. http://dx.doi.org/10.1084/jem.191.7.1247

Ha, S.J., S.N. Mueller, E.J. Wherry, D.L. Barber, R.D. Aubert, A.H. Sharpe, G.J. Freeman, and R. Ahmed. 2008. Enhancing therapeutic vaccination by blocking PD-1-mediated inhibitory signals during chronic infection. *J. Exp. Med.* 205:543–555. http://dx.doi.org/10.1084/jem.20071949

Hamel, K.M., Y. Cao, Y. Wang, R. Rodeghero, T. Kobezda, L. Chen, and A. Finnegan. 2010. B7-H1 expression on non-B and non-T cells promotes distinct effects on T- and B-cell responses in autoimmune arthritis. *Eur. J. Immunol.* 40:3117–3127. http://dx.doi.org/10.1002/eji.201040690

Hensley, L.E., M.A. Smith, J.B. Geisbert, E.A. Fritz, K.M. Daddario-DiCaprio, T. Larsen, and T.W. Geisbert. 2011. Pathogenesis of Lassa fever in cynomolgus macaques. *Virol. J.* 8:205. http://dx.doi.org/10.1186/1743-422X-8-205

Iwai, Y., S. Terawaki, M. Ikegawa, T. Okazaki, and T. Honjo. 2003. PD-1 inhibits antiviral immunity at the effector phase in the liver. *J. Exp. Med.* 198:39–50. http://dx.doi.org/10.1084/jem.20022235

Kägi, D., B. Ledermann, K. Bürki, P. Seiler, B. Odermatt, K.J. Olsen, E.R. Podack, R.M. Zinkernagel, and H. Hengartner. 1994. Cytotoxicity mediated by T cells and natural killer cells is greatly impaired in perforin-deficient mice. *Nature.* 369:31–37. http://dx.doi.org/10.1038/369031a0

Keir, M.E., and A.H. Sharpe. 2005. The B7/CD28 costimulatory family in autoimmunity. *Immunol. Rev.* 204:128–143. http://dx.doi.org/10.1111/j.0105-2896.2005.00242.x

Kim, J.V., S.S. Kang, M.L. Dustin, and D.B. McGavern. 2009. Myelomonocytic cell recruitment causes fatal CNS vascular injury during acute viral meningitis. *Nature.* 457:191–195. http://dx.doi.org/10.1038/nature07591

Kline, J., and T.F. Gajewski. 2010. Clinical development of mAbs to block the PD1 pathway as an immunotherapy for cancer. *Curr. Opin. Investig. Drugs.* 11:1354–1359.

Kunz, S., N. Sevilla, D.B. McGavern, K.P. Campbell, and M.B. Oldstone. 2001. Molecular analysis of the interaction of LCMV with its cellular receptor [α]-dystroglycan. *J. Cell Biol.* 155:301–310. http://dx.doi.org/10.1083/jcb.200104103

Kunz, S., J.M. Rojek, M. Perez, C.F. Spiropoulou, and M.B. Oldstone. 2005. Characterization of the interaction of lassa fever virus with its cellular receptor alpha-dystroglycan. *J. Virol.* 79:5979–5987. http://dx.doi.org/10.1128/JVI.79.10.5979-5987.2005

Lafon, M., F. Mégret, S.G. Meuth, O. Simon, M.L. Velandia Romero, M. Lafage, L. Chen, L. Alexopoulou, R.A. Flavell, C. Prehaud, and H. Wiendl. 2008. Detrimental contribution of the immuno-inhibitor B7-H1 to rabies virus encephalitis. *J. Immunol.* 180:7506–7515.

Latchman, Y.E., S.C. Liang, Y. Wu, T. Chernova, R.A. Sobel, M. Klemm, V.K. Kuchroo, G.J. Freeman, and A.H. Sharpe. 2004. PD-L1-deficient mice show that PD-L1 on T cells, antigen-presenting cells, and host tissues negatively regulates T cells. *Proc. Natl. Acad. Sci. USA.* 101:10691–10696. http://dx.doi.org/10.1073/pnas.0307252101

Lázár-Molnár, E., B. Chen, K.A. Sweeney, E.J. Wang, W. Liu, J. Lin, S.A. Porcelli, S.C. Almo, S.G. Nathenson, and W.R. Jacobs Jr. 2010. Programmed death-1 (PD-1)-deficient mice are extraordinarily sensitive to tuberculosis. *Proc. Natl. Acad. Sci. USA.* 107:13402–13407. http://dx.doi.org/10.1073/pnas.1007394107

Leon, L.R., A.A. White, and M.J. Kluger. 1998. Role of IL-6 and TNF in thermoregulation and survival during sepsis in mice. *Am. J. Physiol.* 275:R269–R277.

Lukashevich, I.S., R. Maryankova, A.S. Vladyko, N. Nashkevich, S. Koleda, M. Djavani, D. Horejsh, N.N. Voitenok, and M.S. Salvato. 1999. Lassa and Mopeia virus replication in human monocytes/macrophages and in endothelial cells: different effects on IL-8 and TNF-alpha gene expression. *J. Med. Virol.* 59:552–560. http://dx.doi.org/10.1002/(SICI)1096-9071(199912)59:4<552::AID-JMV21>3.0.CO;2-A

Matthay, M.A., and R.L. Zemans. 2011. The acute respiratory distress syndrome: pathogenesis and treatment. *Annu. Rev. Pathol.* 6:147–163. http://dx.doi.org/10.1146/annurev-pathol-011110-130158

Mkrtichyan, M., Y.G. Najjar, E.C. Raulfs, M.Y. Abdalla, R. Samara, R. Rotem-Yehudar, L. Cook, and S.N. Khleif. 2011. Anti-PD-1 synergizes with cyclophosphamide to induce potent anti-tumor vaccine effects through novel mechanisms. *Eur. J. Immunol.* 41:2977–2986. http://dx.doi.org/10.1002/eji.201141639

Mueller, S.N., and R. Ahmed. 2009. High antigen levels are the cause of T cell exhaustion during chronic viral infection. *Proc. Natl. Acad. Sci. USA.* 106:8623–8628. http://dx.doi.org/10.1073/pnas.0809818106

Mueller, S.N., V.K. Vanguri, S.J. Ha, E.E. West, M.E. Keir, J.N. Glickman, A.H. Sharpe, and R. Ahmed. 2010. PD-L1 has distinct functions in hematopoietic and nonhematopoietic cells in regulating T cell responses during chronic infection in mice. *J. Clin. Invest.* 120:2508–2515. http://dx.doi.org/10.1172/JCI40040

Nakamoto, N., H. Cho, A. Shaked, K. Olthoff, M.E. Valiga, M. Kaminski, E. Gostick, D.A. Price, G.J. Freeman, E.J. Wherry, and K.M. Chang. 2009. Synergistic reversal of intrahepatic HCV-specific CD8 T cell exhaustion by combined PD-1/CTLA-4 blockade. *PLoS Pathog.* 5:e1000313. http://dx.doi.org/10.1371/journal.ppat.1000313

Nishimura, H., and T. Honjo. 2001. PD-1: an inhibitory immunoreceptor involved in peripheral tolerance. *Trends Immunol.* 22:265–268. http://dx.doi.org/10.1016/S1471-4906(01)01888-9

Nishimura, H., N. Minato, T. Nakano, and T. Honjo. 1998. Immunological studies on PD-1 deficient mice: implication of PD-1 as a negative regulator for B cell responses. *Int. Immunol.* 10:1563–1572. http://dx.doi.org/10.1093/intimm/10.10.1563

Nishimura, H., M. Nose, H. Hiai, N. Minato, and T. Honjo. 1999. Development of lupus-like autoimmune diseases by disruption of the PD-1 gene encoding an ITIM motif-carrying immunoreceptor. *Immunity.* 11:141–151. http://dx.doi.org/10.1016/S1074-7613(00)80089-8

Nishimura, H., T. Okazaki, Y. Tanaka, K. Nakatani, M. Hara, A. Matsumori, S. Sasayama, A. Mizoguchi, H. Hiai, N. Minato, and T. Honjo. 2001. Autoimmune dilated cardiomyopathy in PD-1 receptor-deficient mice. *Science.* 291:319–322. http://dx.doi.org/10.1126/science.291.5502.319

Pascolo, S., N. Bervas, J.M. Ure, A.G. Smith, F.A. Lemonnier, and B. Pérarnau. 1997. HLA-A2.1-restricted education and cytolytic activity of CD8(+) T lymphocytes from β2 microglobulin (β2m) HLA-A2.1 monochain transgenic H-2Db β2m double knockout mice. *J. Exp. Med.* 185:2043–2051. http://dx.doi.org/10.1084/jem.185.12.2043

Phares, T.W., S.A. Stohlman, D.R. Hinton, R. Atkinson, and C.C. Bergmann. 2010. Enhanced antiviral T cell function in the absence of B7-H1 is insufficient to prevent persistence but exacerbates axonal bystander damage during viral encephalomyelitis. *J. Immunol.* 185:5607–5618. http://dx.doi.org/10.4049/jimmunol.1001984

Pircher, H., D. Moskophidis, U. Rohrer, K. Bürki, H. Hengartner, and R.M. Zinkernagel. 1990. Viral escape by selection of cytotoxic T cell-resistant virus variants in vivo. *Nature.* 346:629–633. http://dx.doi.org/10.1038/346629a0

Rodig, N., T. Ryan, J.A. Allen, H. Pang, N. Grabie, T. Chernova, E.A. Greenfield, S.C. Liang, A.H. Sharpe, A.H. Lichtman, and G.J. Freeman. 2003. Endothelial expression of PD-L1 and PD-L2 down-regulates CD8+ T cell activation and cytolysis. *Eur. J. Immunol.* 33:3117–3126. http://dx.doi.org/10.1002/eji.200324270

Shresta, S., K.L. Sharar, D.M. Prigozhin, P.R. Beatty, and E. Harris. 2006. Murine model for dengue virus-induced lethal disease with increased vascular permeability. *J. Virol.* 80:10208–10217. http://dx.doi.org/10.1128/JVI.00062-06

Srikiatkhachorn, A. 2009. Plasma leakage in dengue haemorrhagic fever. *Thromb. Haemost.* 102:1042–1049.

Telcian, A.G., V. Laza-Stanca, M.R. Edwards, J.A. Harker, H. Wang, N.W. Bartlett, P. Mallia, M.T. Zdrenghea, T. Kebadze, A.J. Coyle, et al. 2011. RSV-induced bronchial epithelial cell PD-L1 expression inhibits CD8+ T cell nonspecific antiviral activity. *J. Infect. Dis.* 203:85–94. http://dx.doi.org/10.1093/infdis/jiq020

Topalian, S.L., F.S. Hodi, J.R. Brahmer, S.N. Gettinger, D.C. Smith, D.F. McDermott, J.D. Powderly, R.D. Carvajal, J.A. Sosman, M.B. Atkins, et al. 2012. Safety, activity, and immune correlates of anti-PD-1 antibody in cancer. *N. Engl. J. Med.* 366:2443–2454. http://dx.doi.org/10.1056/NEJMoa1200690

Tracey, K.J., Y. Fong, D.G. Hesse, K.R. Manogue, A.T. Lee, G.C. Kuo, S.F. Lowry, and A. Cerami. 1987. Anti-cachectin/TNF monoclonal antibodies prevent septic shock during lethal bacteraemia. *Nature.* 330:662–664. http://dx.doi.org/10.1038/330662a0

Urbani, S., B. Amadei, D. Tola, G. Pedrazzi, L. Sacchelli, M.C. Cavallo, A. Orlandini, G. Missale, and C. Ferrari. 2008. Restoration of HCV-specific T cell functions by PD-1/PD-L1 blockade in HCV infection: effect of viremia levels and antiviral treatment. *J. Hepatol.* 48:548–558. http://dx.doi.org/10.1016/j.jhep.2007.12.014

Velu, V., K. Titanji, B. Zhu, S. Husain, A. Pladevega, L. Lai, T.H. Vanderford, L. Chennareddi, G. Silvestri, G.J. Freeman, et al. 2009. Enhancing SIV-specific immunity in vivo by PD-1 blockade. *Nature.* 458:206–210. http://dx.doi.org/10.1038/nature07662

Virgin, H.W., E.J. Wherry, and R. Ahmed. 2009. Redefining chronic viral infection. *Cell.* 138:30–50. http://dx.doi.org/10.1016/j.cell.2009.06.036

Wilson, E.B., and D.G. Brooks. 2010. Translating insights from persistent LCMV infection into anti-HIV immunity. *Immunol. Res.* 48:3–13. http://dx.doi.org/10.1007/s12026-010-8162-1